SYNTAPHILIN UBIQUITINATION REGULATES MITOCHONDRIAL DYNAMICS AND TUMOR CELL MOVEMENTS

Jae Ho Seo[1,2], **Ekta Agarwal**[1,2], **Kelly G. Bryant**[1,2], **M. Cecilia Caino**[1,2,*], **Eui Tae Kim**[3], **Andrew V. Kossenkov**[4], **Hsin-Yao Tang**[1,4], **Lucia R. Languino**[1,5], **Dmitry I. Gabrilovich**[1,2], **Andrew R. Cohen**[6], **David W. Speicher**[1,4,7], and **Dario C. Altieri**[1,2]

[1]Prostate Cancer Discovery and Development Program, The Wistar Institute, Philadelphia, PA 19104 USA

[2]Immunology, Microenvironment and Metastasis Program, The Wistar Institute, Philadelphia, PA 19104 USA

[3]Division of Cancer Pathobiology, Children's Hospital of Philadelphia, Philadelphia, PA 19104 USA

[4]Center for Systems and Computational Biology, The Wistar Institute, Philadelphia, PA 19104, USA

[5]Department of Cancer Biology, Kimmel Cancer Center, Thomas Jefferson University, Philadelphia, PA 19107 USA

[6]Department of Electrical and Computer Engineering, College of Engineering, Drexel University, PA 19104 USA

[7]Molecular and Cellular Oncogenesis Program, The Wistar Institute, Philadelphia, PA 19104, USA

Abstract

Syntaphilin (SNPH) inhibits the movement of mitochondria in tumor cells, preventing their accumulation at the cortical cytoskeleton and limiting the bioenergetics of cell motility and invasion. Although this may suppress metastasis, the regulation of the SNPH pathway is not well understood. Using a global proteomics screen, we show that SNPH associates with multiple regulators of ubiquitin-dependent responses and is ubiquitinated by the E3 ligase CHIP (or STUB1) on Lys111 and Lys153 in the microtubule-binding domain. SNPH ubiquitination did not result in protein degradation, but instead anchored SNPH on tubulin to inhibit mitochondrial motility and cycles of organelle fusion and fission i.e. dynamics. Expression of ubiquitination-defective SNPH mutant Lys111→Arg or Lys153→Arg increased the speed and distance traveled

Correspondence to: Dario C. Altieri, M.D., The Wistar Institute Cancer Center, 3601 Spruce Street, Philadelphia, PA 19104, Tel. (215) 495-6970; (215) 495-2638; daltieri@wistar.org.
*Present address: Department of Pharmacology, University of Colorado School of Medicine, Aurora, CO 80045

ONLINE SUPPLEMENTAL MATERIAL

Fig. S1 represents SNPH-associated proteins and modulation of SNPH ubiquitination. Fig. S2 analyzes the stability of SNPH or SNPH mutants in CHX block experiments. Fig. S3 examines 2D tumor chemotaxis and modulation of bioenergetics by SNPH ubiquitination. Fig. S4 characterizes the function of SNPH mutants outside of the MBD in ubiquitination and cell motility. Fig. S5 characterizes the role of mitochondrial fission and Drp1 in mitochondrial trafficking and tumor chemotaxis. Fig. S6 provides a model for ubiquitination-dependent regulation of SNPH in inhibition of mitochondrial trafficking and tumor cell motility.

by mitochondria, repositioned mitochondria to the cortical cytoskeleton, and supported heightened tumor chemotaxis, invasion, and metastasis in vivo. Interference with SNPH ubiquitination activated mitochondrial dynamics, resulting in increased recruitment of the fission regulator dynamin-related protein-1 (Drp1) to mitochondria, and Drp1-dependent tumor cell motility. These data uncover non-degradative ubiquitination of SNPH as a key regulator of mitochondrial trafficking and tumor cell motility and invasion. In this way, SNPH may function as a unique, ubiquitination-regulated suppressor of metastasis.

Keywords

Mitochondria; syntaphilin; tubulin; CHIP; ubiquitin; metastasis

INTRODUCTION

Although most tumors reprogram their metabolism towards glycolysis even when oxygen is present, i.e. the "Warburg effect" (1), there is now mounting evidence that mitochondria continue to play a fundamental role in cancer (2,3). This is especially important in advanced disease, where mitochondrial function has been linked to tumor repopulation after oncogene ablation (4), drug resistance (5), and tumor progression, in vivo (6). In addition, mitochondria have been implicated in tumor cell movements and metastasis (7) through modulation of oxidative metabolism (8), organelle biogenesis (8), buffering of oxidative stress (9), and cycles of organelle fusion and fission, i.e. dynamics (10).

In this context, recent evidence has demonstrated that in response to stress stimuli of the microenvironment, tumor cells reposition mitochondria from their constitutive perinuclear localization to the peripheral (or cortical) cytoskeleton (11). In turn, these cortical mitochondria function as a "spatiotemporal" energy source to fuel membrane lamellipodia dynamics, kinase signaling and actin cytoskeleton remodeling, promoting increased cellular chemotaxis and invasion (11–13).

There are intriguing similarities between these observations in cancer (11–13) and the process of mitochondrial trafficking in neurons, which also repositions mitochondria at sites of high energy demands (14). This suggests that tumors may hijack mitochondrial trafficking as a bioenergetics requirement of cell motility, especially under stress (11), facilitating metastatic dissemination, in vivo. Accordingly, a genome-wide short interfering RNA (shRNA) screen has recently identified syntaphilin (SNPH), a molecule known to inhibit mitochondrial trafficking in neurons (15), as a regulator of tumor cell movements (16). Although considered neuronal-specific, SNPH is, in fact, broadly expressed in cancer, suppresses mitochondrial trafficking to the cortical cytoskeleton, and restricts tumor cell movements and metastasis, in vivo (16). In addition, analysis of genomic databases suggests that SNPH is progressively downregulated or lost during tumor progression, correlating with worse disease outcome (16). How this pathway is regulated, however, has remained elusive.

In this study, we examined a role of SNPH ubiquitination in the control of mitochondrial trafficking and metastasis.

MATERIALS AND METHODS

Cell culture

Prostate adenocarcinoma PC3 cells were obtained from the American Type Culture Collection along with authentication (ATCC, Manassas, VA), and maintained in culture according to the supplier's specifications. Yumm 1.7 cells were a gift from Marcus Bosenberg (Yale University, New Haven, Connecticut). All cell lines were obtained within 5 years, stored in liquid nitrogen and maintained in culture for less than 30 passages. Mycoplasma detection is carried out in our teams by direct PCR amplification of culture supernatants with Bioo Scientific Mycoplasma Primer Sets (cat#375501) and Hot Start polymerase (QIAGEN cat# 203203). Conditioned media used for cell motility assays was prepared from exponentially growing cultures of NIH3T3 cells in DMEM supplemented with 4.5 g/l D-glucose, sodium pyruvate, 10 mM HEPES and 10% FBS for 48 h. Nutrient starvation was carried out in the presence of 0.8% FBS for 16 h.

Antibodies and reagents

An affinity-purified, custom-made rabbit polyclonal antibody against human SNPH (aa 207–221, NEO Group Inc., Cambridge, MA) has been described (17). Antibodies to β-tubulin, β-actin, and Flag were from Sigma. Antibodies to MTC02, Kif2a and Clasp-1 were from Abcam. Antibodies to ubiquitin, VDAC, CHIP, USP7, Ser616-phosphorylated Drp1, Drp1, Rac1 were from Cell Signaling. CHX was from Sigma. An antibody to ubiquitin K11 linkage was from EMD Millipore. Antibodies to ubiquitin K48 and K63 linkages were from Cell Signaling. MitoTracker Green, Phalloidin Alexa488, Mitotracker-Deep Red FM and secondary antibodies for immunofluorescence were from Molecular Probes.

Plasmids, mutagenesis and transfections

The following recombinant proteins were used: UBE1 (E1, UBPBio, cat.n. #B1100), His-UBE2D1 (E2, UBPBio, cat.n. C1400), His-UBE2D3 (E2, UBPBio, cat.n. C1600), His-UBE2E3 (E2, UBPBio, cat.n. C2000), ubiquitin (UBPBio, cat.n. E1100). Recombinant CHIP (Stub1) was purchased from Boston Biochem. A SNPH mutant lacking the kinesin-binding domain (ΔKBD, 337–422 aa) has been characterized previously (16). Ubiquitination-defective SNPH mutants K111R, K153R, K175R, K295R and K415R were generated using Stratagene QuikChange II XL Site-Directed Mutagenesis kit (Agilent Technologies), and confirmed by DNA sequencing. Cells were transfected with 2 μg of pDNA plus 4 μl X-treme gene HP (Roche) for 24 h in complete medium, washed and processed for individual experiments. Adenoviral vectors expressing LacZ, wild type (WT) SNPH, or the various ubiquitination-defective SNPH mutants were produced using Gateway technology (Thermo Fisher Scientific) with pDONR221 vector and recombination into the adenovirus expression vector pAd/CMV/V5-DEST. After digestion with PacI, the individual constructs were transfected in 293A cells for production of adenoviruses after 7 d.

Gene silencing

Gene knockdown experiments by small interfering RNA (siRNA) were carried out as described (16). The following sequences were used: control, ON-TARGET plus non-

targeting siRNA pool (Dharmacon, D-001810), human SNPH siRNA (Dharmacon L-020417 or Santa Cruz sc-41369), Kif2a siRNA (Dharmacon; L-004959–00); Drp1 siRNA (Dharmacon; L-012092–00). USP7 siRNA and CHIP siRNAs were synthesized by Dharmacon. The USP7 siRNA sequence was 5'-AAATTATTCCGCGGCAAA-3' and CHIP siRNA sequence was 5'-CGAGCGCGCAGGAGCTCAA-3'. Tumor cells were transfected with the individual siRNA pools at 30 nM in Lipofectamine RNAiMAX (Invitrogen) at a 1:1 ratio (vol siRNA 20 μM:vol Lipofectamine RNAiMAX). After 48 h, transfected cells were confirmed for protein knockdown by Western blotting, and processed for subsequent experiments. For reconstitution experiments, PC3 cells were transiently silenced for endogenous SNPH expression using siRNA sequence 5'-GCUGCUGACAUUACCAUUAUUUU-3' targeting the 3'UTR of human SNPH mRNA. Cultures were confirmed for silencing of endogenous SNPH expression by Western blotting and transfected with wild type (WT) SNPH or other SNPH mutant constructs followed by functional analyses. Alternatively, PC3 cells stably expressing small interfering RNA (shRNA) targeting the 3'UTR of human SNPH: TRCN 0000147900 and TRCN 0000128545 were used and reconstituted with the various SNPH constructs (17). An empty pLKO-based lentivirus was used as control, and selection of stable clones was carried out in the presence of puromycin (2 μg/ml), as described (17).

Protein analysis

Protein lysates were prepared in RIPA buffer (150 mM NaCl, 1.0% Triton X-100, 0.5% sodium deoxycholate, 0.1% SDS, 50 mM Tris, pH 8.0) in the presence of EDTA-free Protease Inhibitor Cocktail (Roche) and Phosphatase Inhibitor Cocktail (Roche). Equal amounts of protein lysates were separated by SDS gel electrophoresis, transferred to PVDF membranes and incubated with primary antibodies of various specificities. Protein bands were visualized by chemiluminescence. For ubiquitination analysis, cells were washed with 10 mM N-ethylmaleimide (NEM) containing PBS. The cell pellet was lysed by sonication in 50 μl of 2% SDS containing 50 mM Tris-HCl (pH 7.5) and boiled at 95°C in a heat block for 10 min. 950 μl of 50 mM Tris-HCl (pH 7.5) buffer was added to the boiled lysates followed by centrifugation. For immunoprecipitation experiments, aliquots of total cell lysates from control or PC3 transfectants were incubated with anti-Flag M2 affinity agarose gel (sigma) for 16 h at 4°C. The immune complexes were separated by SDS gel electrophoresis, and analyzed by Western blotting. For protein half-life, PC3 cells transfected as indicated in individual experiments were incubated with 100 μg/ml of the protein synthesis inhibitor cycloheximide (CHX), released in complete medium, and aliquots of cell lysates collected at increasing time intervals after release (2–10 h) were analyzed by Western blotting. For in vitro ubiquitination reactions, Flag-SNPH was incubated with E1 (100 nM), E2 (1 μM), E3 (1–2 μM) and Ub (100 μM) in buffer containing 50 mM Tris, pH 8.0, 0.1% Triton X-100, 5 mM MgCl$_2$, 2 mM ATP, 1 mM DTT for 1 h at 37°C. The reaction was terminated with addition of 4X SDS sample buffer and protein bands separated by electrophoresis were visualized by Western blotting.

Proteomics analysis

Immunoprecipitates of WT Flag-SNPH were separated on an SDS-gel for approximately 5 mm followed by fixing and staining with colloidal Coomassie. The entire region of the gel

containing protein was excised and digested with trypsin. Tryptic peptides were analyzed by LC-MS/MS on a Q Exactive Plus mass spectrometer (Thermo Scientific) coupled with a Nano-ACQUITY UPLC system (Waters). Samples were injected onto a UPLC Symmetry trap column (180 μm i.d. × 2 cm packed with 5 μm C18 resin; Waters), and tryptic peptides were separated by RP-HPLC on a BEH C18 nanocapillary analytical column (75 μm i.d. × 25 cm, 1.7 μm particle size; Waters) using a 95-min gradient. Eluted peptides were analyzed in data-dependent mode where the mass spectrometer obtained full MS scans from 400 to 2000 m/z at 70,000 resolution. Full scans were followed by MS/MS scans at 17,500 resolution on the 20 most abundant ions. Peptide match was set as preferred, the exclude isotopes option and charge-state screening were enabled to reject singly and unassigned charged ions. MS/MS spectra were searched using MaxQuant 1.5.2.8 (18) against the UniProt human protein database (August 2015). MS/MS spectra were searched using full tryptic specificity with up to two missed cleavages, static carboxamidomethylation of Cys, and variable oxidation of Met and protein N-terminal acetylation. For identification of ubiquitinated sites, variable modification of diglycine ubiquitin remnant on Lys was also included. Consensus identification lists were generated with false discovery rates of 1% at protein and peptide levels. As cutoff, we focused on candidate SNPH-interacting proteins with at least 2 MS/MS counts in both positive immunoprecipitation experiments, and either showed at least a 5-fold enrichment of both MS protein intensities and MS/MS counts or had no spectra identified in the control samples. Fold-changes were calculated *versus* control values floored to 1,000,000 for Intensity (minimal detected) and 1 for MS/MS counts.

Analysis of bioenergetics

PC3 cells silenced for endogenous SNPH by siRNA and reconstituted with WT SNPH or ubiquitination-deficient SNPH mutants were analyzed for ATP generation (BioChain cat No. Z5030041) or oxygen consumption rate (OCR, ENZO Lifesciences cat. No. ENZ-51045–1), according to the manufacturer's specifications.

Mitochondrial isolation

Mitochondrial fractions were prepared using a mitochondria isolation kit (Fisher Scientific), as described (17).

Mitochondria time-lapse videomicroscopy

Cells (2×10^4) growing on high optical-quality glass bottom 35-mm plates (MatTek Corporation) were treated with 100 nM Mitotracker-Deep Red FM dye for 1 h and imaged with a 63X 1.40NA oil objective on a Leica TCS SP8 X inverted laser scanning confocal microscope. Short duration time-lapse sequences were carried out on a Tokai Hit incubation chamber equilibrated to 37°C and 5% CO_2 bidirectional scanning at 8000 Hz using a resonant scanner. Time lapse was performed for 1000 sec (10 sec per frame). Individual 12-bit images were acquired using a white-light supercontinuum laser (2% at 645 nm) and HyD detectors at 2X digital zoom with a pixel size of 90 nm × 90 nm. A pinhole setting of 1 Airy Units provided a section thickness of 0.896 μm. Each time point was captured as a stack of approximately 11 overlapping sections with a step size of 0.5 μm. At least 5 single cells per condition were collected for analysis. Initial post-processing of the 3D sequences was carried out with Leica LAS X software to create an iso-surface visualization. Time-lapse

sequences were imported into Image J Fiji and individual mitochondria were manually tracked using the Manual Tracking plugin. Mitochondria (approximately 10 mitochondria per cell) were tracked along the stacks until a fusion event prevented continued tracking. The speed and distance for each time interval were used to calculate the mean speed and cumulative distance traveled by each individual mitochondria.

Computational image analysis

Mitochondrial activity was quantified using automated image analysis approaches. Mitochondria were segmented in each image frame and tracked throughout the image sequence. The segmentation and tracking used algorithms previously developed for measuring organelle dynamics (19), utilized from within the LEVER framework for live cell microscopy image analysis (20–22). Briefly, the segmentation uses an adaptive thresholding on the 3-D image data, followed by a connected component analysis to identify individual mitochondria. A single segmentation parameter specifying the expected minimum object radius is required, here set at 0.5 μm for all of the image data processed. Tracking is done using the MAT (multitemporal association tracking) algorithm (19,23) that uses a minimum-spanning tree approach to solve the data association problem in polynomial time across a time window here set at 3 frames into the future. No parameters beyond the minimum expected object radius are required for the tracking algorithm. Following segmentation and tracking, we identify fission and fusion events from the mitochondrial tracking results as follows. Tracks lasting a minimum number of frames (here set at 3 frames) that originate (or terminate) after the first frame of the video are considered to have originated from a fission (or fusion) event. For each movie, we normalize the number of fission and fusion events using the number of foreground voxels identified in the first frame of the image sequence. The result is a count of the fission and fusion events per frame per voxel for each movie.

Cortical mitochondria and total mitochondrial mass quantification

Mitochondria/F-actin composite images were analyzed in ImageJ, as described (11). Briefly, the F-actin channel was used to manually label the cell boundary and a belt extending from the boundary towards the inside of the cell was marked as "cortical mask". This cortical mask was subsequently applied to the mitochondrial channel to measure intensity at the cortical region, and normalized to total mitochondrial intensity per cell and cell area. For quantification of total mitochondrial mass, composite images were analyzed in ImageJ. The cell border was manually traced on the F-actin channel and this "cell mask" was subsequently applied to the mitochondria channel to measure the total mitochondria signal per cell. Maximum intensity was monitored to ensure no pixel saturation (e.g. Max intensity <256 for 8-bit images). Mitochondrial mass was normalized to total cell area. A minimum of 30 cells was analyzed in each independent experiment to obtain mean values.

Immunofluorescence

Cells were fixed in formalin/PBS (4% final concentration) for 15 min at 22°C, permeabilized in 0.1% Triton X-100/PBS for 5 min, washed, and incubated in 5% normal goat serum (NGS, Vector Labs) diluted in 0.3 M glycine/PBS for 60 min. Primary antibodies against Tom20 (diluted 1:300), β-tubulin (diluted 1:200), SNPH (diluted 1:500) or MTC02 (diluted 1:500) were added in 5% NGS/0.3 M glycine/PBS and incubated for 18 h at 4°C.

After 3 washes in PBS, secondary antibodies conjugated either to Alexa488, TRITC or Alexa633 were diluted 1:500 in 5% NGS/0.3 M glycine/PBS and added to cells for 1 h at 22°C. Where indicated, F-actin was stained with phalloidin Alexa488 (1:200 dilution) for 30 min at 22°C. Slides were washed and mounted in DAPI-containing Prolong Gold mounting medium (Invitrogen). At least 7 random fields were analyzed by fluorescence microscopy in a Nikon i80 microscope.

2D tumor chemotaxis

Experiments were carried out as described (11). Briefly, 2×10^4 PC3 or Yumm 1.7 cells were seeded in 4-well Ph+ Chambers (Ibidi) in complete medium and allowed to attach overnight. Videomicroscopy was performed over 10 h, with a time-lapse interval of 10 min. Stacks were imported into Image J Fiji for analysis. Images were aligned according to subpixel intensity registration with the StackReg plugin for Image J Fiji (24). At least 25–30 cells were tracked using the Manual Tracking plugin for Image J Fiji, and the tracking data were exported into the Chemotaxis and Migration Tool v2.0 (Ibidi) for graphing and calculation of mean and standard deviation of speed, accumulated distance and Euclidean distance of movement.

Tumor cell invasion

Experiments were carried out essentially as described (16) using Growth Factor Reduced Matrigel-coated 8 μm PET transwell chambers (Corning). Tumor cells were seeded in duplicates onto the coated transwell filters at a density of 1×10^5 cells/well in medium containing 0.1% BSA and conditioned media from NIH3T3 was placed in the lower chamber as chemoattractant. Cells were allowed to invade for 16–24 h, non-invading cells were scraped off the top side of the membranes and the invasive cells on the transwell insert were fixed in methanol. Membranes were mounted in medium containing DAPI (Vector Labs) and analyzed by fluorescence microscopy. Five random fields at 10X magnification were collected for each membrane. Digital images were batch imported into ImageJ Fiji, thresholded and analyzed with the Analyze particles function. Experiments were repeated three times.

Animal studies

Studies involving rodents were carried out in accordance with the Guide for the Care and Use of Laboratory Animals of the National Institutes of Health (NIH). Protocols were approved by the Institutional Animal Care and Use Committee (IACUC) of The Wistar Institute (Protocol # 112625). For a syngeneic model of metastasis, Yumm 1.7 cells stably expressing mCherry (17) were transiently transfected with pCMV6 vector, or cDNA encoding WT SNPH or ubiquitination-defective SNPH mutant K111R or K153R mutant and selected with G418 at 400 μg/ml for 15 d. Stably transfected cells (3.5×10^5) were injected into the flanks of syngeneic 8-week-old male C57BL6/NCr mice (NCI Inbred mice, Charles River Strain code #556). One week later, tumor cells disseminated to lungs were identified and quantitated based on expression of the mCherry transgene by immunohistochemistry (IHC).

IHC

Lungs were fixed in neutral formalin (Fisher Scientific, SF93–4) for 36 h, transferred to 70% ethanol for 3 d, and then paraffin-embedded. Five-μm sections were stained with a rabbit anti-mCherry polyclonal antibody (Novus, NBP2–25157) as follows. Slides were warmed at 50°C for 30 min; deparaffinized in xylene for 20 min, then xylene/ethanol 1:1 for 5 min; and rehydrated in alcohol series (100%, 95%, 90%, 70%, 50%, 30% ethanol and dH_2O, 5 min each). Antigen retrieval was done in citrate-based solution (Vector Laboratories, H-3300) at pH 6.0 in a pressure cooker for 5 min, followed by cooling to room temperature. Next, slides were washed once in PBS for 5 min and incubated in 3% hydrogen peroxide for 20 min. Slides were then washed 3 times with PBS (5 minutes each) and blocked in 10% normal goat serum/PBS for 1 h at room temperature. The primary antibody was diluted 1:500 in 10% normal goat serum/PBS and incubated in a humidified chamber overnight. The next day, slides were washed 3 times with PBS for 5 min each, incubated with anti-rabbit HRP-labeled polymer (Dako, K4002) at 22°C for 30 min, and washed 3 times with PBS for 5 min each. Slides were developed with a DAB+ substrate chromogen system (Dako, K3467) for 30 min, rinsed in dH_2O, and stained with Mayer's hematoxylin solution (Sigma-Aldrich, MHS16) for 10 sec. Slides were dehydrated in dH_2O and serial ethanol rinses of 5 min each, immersed in xylene for 15 min and mounted with Permount mounting medium (Fisher Scientific, SP15–100).

Quantification of disseminated tumor cells to the lungs

Nine lungs per group were examined for the presence of mCherry^{+} cells using a Nikon i80 upright microscope. An average of 5–9 individual microscopy fields were quantified per lung condition and each mCherry[+] cell was photographed at 40X magnification and manually counted using Image J software. For each animal, the average number of mCherry^{+} cells per lung was calculated and represented.

Statistical analysis

Data expressed as mean±SD of multiple independent experiments or replicates of representative experiments out of a minimum of two or three independent determinations. Two-tailed Student's *t* test or Wilcoxon rank sum test was used for two-group comparative analyses. For multiple-group comparisons, including quantification of disseminated tumor cells, ANOVA with Bonferroni's post-test was used to compare the means between the groups and derived pairwise comparison's p values. All statistical analyses were performed using GraphPad software package (Prism 6.0) for Windows. A p value of <0.05 was considered as statistically significant.

RESULTS

Proteomics screening of SNPH-associated molecules

We began this study by conducting a proteomics screen to identify SNPH-associated proteins in model prostate adenocarcinoma PC3 cells (16). Using predetermined mass spectrometry cutoff parameters (see Materials and Methods), we identified 217 putative interacting targets (Fig. S1A), and the top 50 hits were further examined for pathway

enrichment (Fig. S1A, Table S1). In this analysis, protein ubiquitination was identified as the most represented pathway in SNPH-associated molecules ($p=1\times10^{-19}$; FDR, 0%) with a total of 34 proteins (Table S1). Other SNPH-associated proteins clustered in RNA translation ($p=2\times10^{-19}$; FDR, 0%) with 29 proteins, DNA damage response and G2/M checkpoint ($p=5\times10^{-7}$; FDR, 0%) with 13 proteins, cytoskeleton ($p=4\times10^{-5}$; FDR, 0.07%) with 17 proteins, mitochondrial function ($p=0.0016$; FDR, 1.58%) with 7 proteins, and endocytosis signaling ($p=7\times10^{-5}$; FDR, 0.12%) with 6 proteins (Fig. 1A, Table S1). As the most abundant class of SNPH-associated molecules, we next focused on protein ubiquitination.

SNPH ubiquitination

Consistent with the data above, SNPH immune complex(es) precipitated from PC3 cells included heavily ubiquitinated proteins, by Western blotting (Fig. 1B). Using ubiquitin-specific antibodies, most of SNPH ubiquitination under these conditions involved Lys63 linkages (Fig. 1C). Lys48 linkages were predominantly involved in the formation of higher molecular weight SNPH (poly)ubiqitination, whereas Lys27 linkages were not associated with SNPH (Fig. 1C). Based on these findings, we next used LC-MS/MS to identify potential ubiquitinated SNPH residues. Mass spectrometry analysis of tryptic digests of Flag-SNPH immunoprecipitated from PC3 cells revealed partial ubiquitination of K111, K175, K295 and K415 (Fig. 1D). An additional residue, K153 was reported as a site of SNPH ubiquitination in an independent global ubiquitome screen (25). Although modification of that residue was not detected in our analysis possibly because of sparse peptide coverage in the tryptic digests, we further pursued K153 as a putative SNPH ubiquitination site. In the predicted SNPH structure, K111 and K153 localize in the microtubule-binding domain (MBD), K175 and K295 in the inter-domain region upstream of the LC8-binding domain and K415 in the kinesin-binding domain (KBD) (Fig. S1B). To begin validating these results, we first focused on SNPH ubiquitination sites in the MBD, K111 and K153 (Fig. S1B). Accordingly, SNPH mutant K111R or K153R immunoprecipitated from PC3 cells showed significantly reduced ubiquitin labeling, compared to wild type (WT) SNPH (Fig. 1E).

Stress-dependent regulation of SNPH ubiquitination

Next, we asked whether stress conditions typical of the tumor microenvironment affected SNPH ubiquitination. Exposure of PC3 cells to nutrient deprivation (0.8% FBS for 16 h) increased SNPH ubiquitination (Fig. S1C), compared to control cultures. Accordingly, nutrient-deprived PC3 cultures exhibited markers of cellular starvation, including increased phosphorylation of AMPK (Thr172), its downstream substrate acetyl-CoA carboxylase (ACC, Ser 79) and the autophagy regulator ULK1 (Ser555) (Fig. S1D). Conversely, exposure of PC3 cells to hypoxia (1% O_2) or oxidative stress (oxidant paraquat, PQ) reduced SNPH ubiquitination, compared to control (Fig. S1E).

Non-degradative SNPH ubiquitination by CHIP and USP7

We next sought to identify the regulators of SNPH ubiquitination. Potential candidate SNPH-associated proteins in this pathway included the chaperone-regulated E3 ligase, C terminus of HSC70-Interacting Protein (CHIP), also known as STUB1, and the deubiquitinase, USP7 (Fig. S1A, Table S1). Accordingly, WT SNPH or SNPH mutant

K111R or K153R readily associated with CHIP and USP7 in co-immunoprecipitation experiments from PC3 cells (Fig. 2A). Functionally, silencing CHIP by small interfering RNA (siRNA) (Fig. S2A) suppressed SNPH ubiquitination, compared to control transfectants (Fig. 2B). Reciprocally, siRNA silencing of USP7 (Fig. S2A) or pharmacologic inhibition of USP7 with the small molecule antagonist P5091 increased ubiquitination of immunoprecipitated SNPH, in vivo (Fig. 2C). We next reconstituted an in vitro SNPH ubiquitination reaction using recombinant proteins. In these experiments, the addition of recombinant CHIP plus UBE2D1 (UbcH5a, E2) and ubiquitin (E1) resulted in direct SNPH ubiquitination, in vitro (Fig. 2D). In contrast, UBE2E3 (UbcH9, E2) or UBE2D3 (UbcH5c, E2) was ineffective (Fig. 2D). To further validate a direct role of CHIP in SNPH ubiquitination, we next transfected serum-deprived PC3 cells with WT CHIP or a CHIP H260Q mutant, defective in E3 ligase function. Flag SNPH immunoprecipitated from these cells (Fig. S2B) was heavily ubiquitinated in the presence of WT CHIP, whereas expression of CHIP H260Q mutant inhibited SNPH ubiquitination to the levels of non-transfected cells (Fig. 2E).

Next, we asked whether CHIP ubiquitination of SNPH affected protein stability. In cycloheximide block experiments, there was no difference in the half-life of WT SNPH or the ubiquitination-defective SNPH mutant K111R and K153R (Fig. S2C and D). Similarly, siRNA silencing of CHIP or USP7 (Fig. S2A) did not affect SNPH half-life in CHX block experiments (Fig. S2E and F). Conversely, siRNA silencing of CHIP increased the stability of RUNX1 used as control protein in CHX block experiments (Fig. S2E and F). Finally, small molecule inhibitors of proteasomal (MG132) or lysosomal (Bafilomycin A1, BafA1) functions did not affect steady-state levels of endogenous SNPH or Flag-SNPH transfected in PC3 cells (Fig. S2G). We conclude from these results that CHIP ubiquitination does not affect SNPH stability in tumor cells.

SNPH ubiquitination regulates tubulin binding

Our proteomics screen identified tubulin-binding proteins that co-associate with SNPH, including kinesin 13 family members of tubulin depolymerases, Kif2a and Kif2c, and the microtubule-stabilizing protein, Clasp1 (Fig. S1A). Consistent with these results, WT or ubiquitination-defective SNPH mutant K111R or K153R SNPH immunoprecipitated from PC3 cells contained co-associated Kif2a and Clasp1 (Fig. 2A). In these experiments, SNPH mutant K111R or K153R showed considerably reduced co-association with tubulin, compared to WT SNPH (Fig. 2A). To test a potential role of SNPH ubiquitination in direct tubulin binding, we next depleted Kif2a by siRNA (Fig. 2F). In the absence of Kif2a, binding of SNPH mutant K111R to tubulin was considerably reduced, compared to WT SNPH (Fig. 2F). Similar results were obtained with a SNPH double mutant K111R/K153R, which also showed reduced co-association with tubulin after Kif2a silencing (Fig. 2F). As an independent approach, we next used a SNPH mutant lacking the KBD, and therefore defective in Kif2a binding. In co-immunoprecipitation experiments, tubulin association with KBD-SNPH was significantly reduced compared to WT SNPH (Fig. 2G), reinforcing a role of Kif2a in tubulin recognition in the SNPH complex. Under these conditions, ubiquitination-defective KBD-SNPH mutant K111R or K153R minimally co-associated with tubulin (Fig. 2G). Finally, we carried out similar experiments in nutrient-deprived cells,

a condition that increases SNPH ubiquitination (Fig. S1C). In these studies, nutrient deprivation increased tubulin binding to KBD-SNPH, in vivo, whereas immunoprecipitated KBD-SNPH mutant K111R or K153R showed minimal association with tubulin (Fig. 2G).

SNPH ubiquitination controls mitochondrial trafficking

To test the implications of SNPH ubiquitination, we next used Yumm 1.7 melanoma cells, which express low levels of endogenous SNPH (17). Expression of ubiquitination-defective SNPH mutant K111R or K153R was sufficient to increase the speed (Fig. 3A and B), and distance traveled by individual mitochondria in Yumm 1.7 cells (Fig. 3B), compared to WT SNPH. Next, we silenced endogenous SNPH in PC3 cells by siRNA and reconstituted the cultures with different SNPH constructs. Consistent with previous data (16), siRNA silencing of SNPH in PC3 cells was sufficient to drive the active repositioning of mitochondria from a perinuclear localization to infiltrate the cortical cytoskeleton (Fig. 3C). Reconstitution of these cells with WT SNPH suppressed organelle trafficking and maintained a perinuclear distribution of mitochondria (Fig. 3C). Conversely, expression of ubiquitination-defective SNPH mutant K111R or K153R restored mitochondrial infiltration to the cortical cytoskeleton (Fig. 3C). We next quantified mitochondrial trafficking in these conditions, and we found that expression of WT SNPH in siRNA-silenced cells blocked the cortical infiltration of mitochondria to levels of control transfectants (Fig. 3D and E). Conversely, expression of SNPH mutant K111R or K153R sustained mitochondrial trafficking to the cortical cytoskeleton, indistinguishably from SNPH-depleted cells (Fig. 3D and E). Similar results were obtained in Yumm 1.7 cells, where reconstitution of siRNA-silenced cultures with WT SNPH suppressed mitochondrial infiltration to the cortical cytoskeleton, whereas SNPH mutants K111R or K153R restored mitochondrial motility (Fig. 3F).

Regulation of tumor chemotaxis by SNPH ubiquitination

In agreement with previous results (12,16,26), siRNA silencing of endogenous SNPH increased 2D chemotaxis of PC3 cells, characterized by heightened speed of cell movements and longer distance traveled by individual cells (Fig. 4A and B). Expression of WT SNPH suppressed 2D chemotaxis, whereas reconstitution with SNPH mutant K111R or K153R restored the increased speed of cell movements and distance traveled by individual cells (Fig. 4A and B). Biochemically, this response was associated with increased phosphorylation of mTOR and Akt kinases (11), as well as GTPase Rac1 (Fig. 4C). In contrast, reconstitution of these cells with WT SNPH did not affect kinase or Rac1 activation (Fig. 4C). Similar results were obtained with Yumm 1.7 cells, where expression of ubiquitination-defective SNPH K111R or K153R promoted 2D chemotaxis (Fig. S3A and B), and increased phosphorylation of mTOR and Akt (Fig. 4D). Finally, inhibition of SNPH ubiquitination by siRNA knockdown of CHIP increased tumor chemotaxis with greater speed and distance traveled by individual cells (Fig. 4E and F). Conversely, siRNA silencing of USP7 suppressed 2D tumor chemotaxis (Fig. 4E and F).

A pool of SNPH localized to the inner mitochondrial membrane affects bioenergetics in tumor cells (17), and the role of ubiquitination in this response was next investigated. Consistent with earlier findings (17), siRNA silencing of endogenous SNPH in PC3 cells

reduced ATP production (Fig. S3C) and oxygen consumption (Fig. S3D), a marker of oxidative phosphorylation. Reconstitution of these cells with WT SNPH or SNPH mutant K111R or K153R restored ATP production and oxygen consumption (Fig. S3C and D), demonstrating that CHIP ubiquitination does not affect bioenergetics. Based on these data, we next looked at a potential effect on tumor cell proliferation. Also consistent with earlier results, depletion of endogenous SNPH in tumor cells (Fig. S3E) was associated with reduced cell proliferation (Fig S3F), potentially reflecting decreased ATP production (Fig. S3C) and higher ROS generation. Conversely, reconstitution of SNPH-depleted cells with adenovirus encoding WT SNPH or SNPH mutant K111R or K153R (Fig. S3E) comparably restored tumor cell proliferation (Fig. S3F).

SNPH ubiquitination controls tumor cell invasion and metastasis, in vivo

Consistent with increased chemotaxis (Fig. 4A and B), expression of ubiquitination-defective SNPH mutant K111R or K153R, alone or as a double mutant (DM), promoted greater invasion of PC3 cells across Matrigel-coated inserts, compared to control transfectants (Fig. 5A and B). Instead, expression of WT SNPH suppressed tumor cell invasion (Fig. 5A and B). When analyzed in reconstitution experiments, knockdown of SNPH also increased tumor cell invasion, in a reaction suppressed by WT SNPH, but restored by K111R or K153R mutant (Fig. 5C). Comparable results were obtained by targeting the regulators of SNPH ubiquitination. In these experiments, siRNA silencing of CHIP increased tumor cell invasion, whereas USP7 knockdown was profoundly inhibitory (Fig. S4A and 5D).

We next asked whether ubiquitination of the SNPH residues outside the MBD (Fig. S2B) influenced tumor cell invasion. For these experiments, we transduced PC3 cells with adenovirus constructs encoding Flag-tagged SNPH mutant K175R, K295R or K415R, plus K111R and K153R used as control (Fig. S4B). Consistent with the results of the proteomics screen, Flag-tagged SNPH mutant K175R, K295R or K415R precipitated from PC3 cells showed decreased ubiquitination, comparably to immunoprecipitated K111R or K153R (Fig. S4C). Functionally, expression of ubiquitination-defective SNPH mutants, including K175R, K295R or K415R increased 2D chemotaxis, resulting in greater speed of cell movements and longer distance traveled by individual cells (Fig. S4D). Similar results were obtained in reconstitution experiments, where transfection of each ubiquitination-defective SNPH mutant restored tumor cell invasion in siRNA-silenced cells, similar to SNPH depletion (Fig. S4E). Finally, we asked whether SNPH ubiquitination was important for metastasis, in vivo. In these experiments, stable transfection of Yumm 1.7 cells with WT SNPH suppressed metastatic seeding to the lung in a syngeneic mouse model of disseminated melanoma, compared to control transfectants (Fig. 5E and F). Conversely, expression of ubiquitination-defective SNPH mutant K111R or K153R significantly increased the frequency of disseminated tumor cells (DTC) to the lung, compared to control transfectants (Fig. 5E and F).

SNPH ubiquitination regulates mitochondrial dynamics

We next used a novel tracking method based on the MAT (multitemporal association tracking) algorithm (19,23) with a minimum-spanning tree approach (see Materials and

Methods) to quantify the impact of SNPH ubiquitination on mitochondrial dynamics (Fig. 6A). In these experiments, we observed that transfection of WT SNPH in Yumm 1.7 cells profoundly suppressed cycles of mitochondrial fusion and fission, compared to control transfectants (Fig. 6B and C). Conversely, expression of ubiquitination-defective SNPH mutant K111R or K153R restored mitochondrial dynamics in these settings, comparably to control cultures (Fig. 6B and C). Furthermore, expression of SNPH mutant K111R or K153R resulted in recruitment of the fission regulator, Dynamin-Related Protein-1 (Drp1) to mitochondria, as well as increased Drp1 phosphorylation on the activating residue, S616 (Fig. 6D). Conversely, WT SNPH did not induce mitochondrial recruitment of Drp1 or Drp1 phosphorylation (Fig. 6D). Total Drp1 levels and S616-phosphorylated Drp1 expression in total cell extracts was not affected (Fig. 6D). Similar results were obtained after siRNA silencing of SNPH, which induced recruitment of Drp1 to mitochondria, and its phosphorylation on S616 (Fig. 6E). siRNA silencing of CHIP also caused increased phosphorylation of Drp1 on S616 and reduced phosphorylation of Drp1 on the inhibitory site, S637, whereas USP7 silencing had the opposite effect, decreasing Drp1 phosphorylation on S616 and upregulating the levels of S637-phosphorylated Drp1 (Fig. 6F).

Requirement of Drp1 for mitochondrial trafficking and tumor cell movements

Next, we asked if modulation of mitochondrial dynamics by SNPH ubiquitination was important for organelle trafficking and tumor cell motility. siRNA silencing of Drp1(Fig. S5A) suppressed mitochondrial motility in Yumm 1.7 cells (Fig. S5B), restricting the distance traveled by individual mitochondria as well as the speed of organelle movements (Figure S5C). This was associated with inhibition of PC3 cell invasion across Matrigel-coated inserts (Fig. 7A and B). Consistent with a role of SNPH in this response, expression of GTPase-defective (GD) Drp1 mutant (Fig. S5D) prevented the increase in PC3 cell invasion after SNPH knockdown (Fig. 7C). To test whether this pathway involved SNPH ubiquitination, we next quantified mitochondrial movements in Drp1-silenced Yumm 1.7 cells expressing WT SNPH or SNPH mutant K111R (Fig. S5E). Drp1 knockdown suppressed the increased mitochondrial speed (Fig. 7D and E) and distance traveled by individual mitochondria (Fig. S5F) in the presence of SNPH mutant K111R. Silencing of Drp1 further reduced residual mitochondrial movements in cells expressing WT SNPH, affecting both mitochondrial speed (Fig. 7E, Fig. S5G) and distance traveled (Fig. S5F). Similar results were obtained in experiments of 2D chemotaxis, where depletion of Drp1 suppressed the increased speed of migration and distance traveled by individual cells in the presence of SNPH mutant K111R (Fig. 7F and G). In contrast, Drp1 knockdown minimally affected residual cell motility in the presence of WT SNPH (Fig. 7F and G).

DISCUSSION

In this study, we have shown that Syntaphilin (SNPH) (14) is ubiquitinated in tumor cells on multiple lysine residues by the E3 ligase, CHIP under conditions of microenvironment stress. Instead of proteasomal degradation, CHIP ubiquitination enables a direct association of SNPH with tubulin, which is required to inhibit mitochondrial movements (Fig. S6). Interference with SNPH ubiquitination increases mitochondrial trafficking to the cortical

cytoskeleton, restores mitochondrial dynamics and fuels tumor cell movements with heightened chemotaxis, invasion and metastasis, in vivo. Mechanistically, SNPH ubiquitination regulates the recruitment of the fission regulator, Drp1 to mitochondria, which is required to support organelle trafficking to the cortical cytoskeleton and tumor chemotaxis (Fig. S6).

Although first described in neurons as a mechanism to concentrate an efficient bioenergetics source at sites with high energy demands (15), mitochondrial trafficking may extend beyond the CNS, and provide a localized energy source to support membrane dynamics and directional migration in disparate cell types (26,27). A similar model has been proposed in cancer, where exploitation of "neuronal" regulators of mitochondrial motility, including SNPH (16), repositions mitochondria to the cortical cytoskeleton, fueling tumor cell invasion (11), and metastasis (16). Here, an unbiased proteomics screen uncovered regulators of protein ubiquitination as the most abundant class of SNPH-associated molecules in cancer, and identified CHIP, or STUB1 (28) as a SNPH E3 ubiquitin ligase, in vivo. Although the role of post-translational modifications in mitochondrial trafficking has not been widely studied (29), CHIP has attracted attention for a dual regulation of protein homeostasis in cooperation with Heat Shock Protein (Hsp) chaperones, especially Hsp70 and Hsp90 (30), and ubiquitination-coupled proteasomal destruction of protein targets (31). This pathway may contribute to aging (32) and various mechanisms of tumor suppression through inhibition of cancer metabolism (33), androgen receptor transcription (34), and NFκB signaling (35). The data here that CHIP ubiquitination enables the function of SNPH in restricting tumor cell movements is consistent with the proposed tumor suppressor function, and may provide a mechanistic basis for other data that CHIP ubiquitination inhibits metastasis in vivo (36), and further reduces tumor cell motility via proteasomal degradation of integrin-linked kinase (37).

Unexpectedly, we found that CHIP ubiquitination of SNPH does not couple to proteasomal destruction. Experimentally, there was no difference in the half-life of WT or ubiquitination-defective SNPH mutants, and proteasome inhibitors or CHIP silencing had no effect on SNPH stability. There is precedent for non-degradative pathways of CHIP ubiquitination. For instance, CHIP ubiquitination controls the subcellular shuttling of the transcriptional co-repressor, Daxx independently of proteasomal degradation (38), and participates in epigenetics control of gene expression via increased stability of the sirtuin family member, SirT6 (39). Biochemically, these non-degradative responses have been ascribed to non-canonical ubiquitin modification(s), independently of Lys40 (40), and data presented here suggest that most SNPH ubiquitination involves Lys63 linkages, with higher molecular weight (poly)ubiquitination moieties implicating Lys48.

Instead of proteasomal degradation, CHIP ubiquitination of SNPH on K111 and K153 in the MBD enabled direct binding to tubulin, a requisite to suppress mitochondrial movements and organelle dynamics (16). This is reminiscent of other non-degradative ubiquitination signals that mediate protein-protein interactions, in particular during immune and inflammatory responses (41). Conversely, other molecules found in the SNPH complex(es) bind tubulin, including members of the kinesin-13 family of microtubule depolymerases, Kif2a and Kif2c (42), and, conversely, a microtubule-stabilizing protein, Clasp1 (43).

Whether a similar recruitment of tubulin-binding proteins occurs in non-transformed cells, including neurons (14), is unknown. However, for the role of Kif2a and Clasp1 in microtubule dynamics (44), it is possible that their association with SNPH controls the assembly of a stable microtubule track, potentially required for efficient mitochondrial transfer (45). In addition, we found that other SNPH lysine residues outside the MBD (K175, K295 and K415) are ubiquitinated, in vivo, and relevant for tumor cell motility (see below). The role of these additional SNPH ubiquitination sites remains to be fully elucidated, but it could be speculated that their post-translational modification(s) contributes to stabilize SNPH-microtubule interaction mediated by the MBD.

Mimicking the effect of SNPH depletion (16), interference with SNPH ubiquitination was sufficient to reposition mitochondria to the cortical cytoskeleton of tumor cells through faster speed of organelle movements and longer distance traveled. Consistent with a model of regional mitochondrial bioenergetics to sustain tumor cell movements, loss of SNPH ubiquitination was associated with Akt and mTOR phosphorylation, heightened chemotaxis and invasion, and formation of lung metastasis, in vivo. Together, these data point to SNPH as a novel ubiquitination-regulated *metastasis suppressor* (16), and, accordingly, pharmacologic or genetic targeting of the USP7 deubiquitinase abrogated mitochondrial movements, restricted chemotaxis and blocked tumor cell invasion. Although this is consistent with an oncogenic function of USP7 and actionable therapeutic target (46), a role of this pathway in tumor cell motility has not been previously demonstrated.

Mechanistically, CHIP ubiquitination of SNPH regulated mitochondrial dynamics, suppressing cycles of organelle fission and fusion in tumor cells (47). In contrast, interference with SNPH ubiquitination restored mitochondrial dynamics and promoted recruitment of S616-phosphorylated Drp1 to mitochondria (47). These data mirror earlier findings, where SNPH depletion resulted in heightened mitochondrial dynamics, with increased frequency of fusion and fission cycles in tumor cells (16). As a regulator of organelle size, shape and mass (47), there is evidence that mitochondrial dynamics is exploited in cancer (48), and may contribute to tumor cell invasion (10). Whether this predominantly involves fusion or fission has been debated (48). The data here that active Drp1 is required for mitochondrial trafficking and tumor chemotaxis are consistent with other findings that NIK signaling repositions mitochondria to the cortical cytoskeleton in a Drp1-dependent manner (26), and that mitochondrial fission enables faster transfer of mitochondria along microtubules in tumor cells (16). How mitochondrial fission couples to SNPH levels (16) or SNPH ubiquitination (this study) has not been determined. One possibility is that this response involves cytoskeletal remodeling at the mitochondrial interface (49), or mTOR activation (50), processes potentially linked to SNPH function in cancer (16).

In summary, we identified a critical post-translational modification, i.e. ubiquitination that enables a potent, *metastasis-suppressor* function of SNPH. The results reinforce the general exploitation of mitochondrial dynamics (48), including organelle trafficking (11–13) for tumor cell motility, and anticipate its potential as an actionable therapeutic target in metastatic disease (7).

Supplementary Material

Refer to Web version on PubMed Central for supplementary material.

ACKNOWLEDGMENTS

LITERATURE CITED

1. Ward PS , Thompson CB . Metabolic reprogramming: a cancer hallmark even warburg did not anticipate. Cancer Cell 2012;21:297–30822439925

2. Zong WX , Rabinowitz JD , White E . Mitochondria and Cancer. Mol Cell 2016;61:667–7626942671

3. Vyas S , Zaganjor E , Haigis MC . Mitochondria and Cancer. Cell 2016;166:555–6627471965

4. Viale A , Pettazzoni P , Lyssiotis CA , Ying H , Sanchez N , Marchesini M , Oncogene ablation-resistant pancreatic cancer cells depend on mitochondrial function. Nature 2014;514:628–3225119024

5. Zhang G , Frederick DT , Wu L , Wei Z , Krepler C , Srinivasan S , Targeting mitochondrial biogenesis to overcome drug resistance to MAPK inhibitors. J Clin Invest 2016;126:1834–5627043285

6. Sellers K , Fox MP , Bousamra M , Slone SP , Higashi RM , Miller DM , Pyruvate carboxylase is critical for non-small-cell lung cancer proliferation. J Clin Invest 2015;125:687–9825607840

7. Steeg PS . Targeting metastasis. Nat Rev Cancer 2016;16:201–1827009393

8. LeBleu VS , O'Connell JT , Gonzalez Herrera KN , Wikman H , Pantel K , Haigis MC , PGC-1alpha mediates mitochondrial biogenesis and oxidative phosphorylation in cancer cells to promote metastasis. Nat Cell Biol 2014;16:992–100325241037

9. Porporato PE , Payen VL , Perez-Escuredo J , De Saedeleer CJ , Danhier P , Copetti T , A mitochondrial switch promotes tumor metastasis. Cell Rep 2014;8:754–6625066121

10. Zhao J , Zhang J , Yu M , Xie Y , Huang Y , Wolff DW , Mitochondrial dynamics regulates migration and invasion of breast cancer cells. Oncogene 2013;32:4814–2423128392

11. Caino MC , Ghosh JC , Chae YC , Vaira V , Rivadeneira DB , Faversani A , PI3K therapy reprograms mitochondrial trafficking to fuel tumor cell invasion. Proc Natl Acad Sci U S A 2015;112:8638–4326124089

12. Cunniff B , McKenzie AJ , Heintz NH , Howe AK . AMPK activity regulates trafficking of mitochondria to the leading edge during cell migration and matrix invasion. Mol Biol Cell 2016;27:2662–7427385336

13. Mills KM , Brocardo MG , Henderson BR . APC binds the Miro/Milton motor complex to stimulate transport of mitochondria to the plasma membrane. Mol Biol Cell 2016;27:466–8226658612

14. Birsa N , Norkett R , Higgs N , Lopez-Domenech G , Kittler JT . Mitochondrial trafficking in neurons and the role of the Miro family of GTPase proteins. Biochem Soc Trans 2013;41:1525–3124256248

15. Sheng ZH . Mitochondrial trafficking and anchoring in neurons: New insight and implications. J Cell Biol 2014;204:1087–9824687278

16. Caino MC , Seo JH , Aguinaldo A , Wait E , Bryant KG , Kossenkov AV , A neuronal network of mitochondrial dynamics regulates metastasis. Nat Commun 2016;7:1373027991488

17. Caino MC , Seo JH , Wang Y , Rivadeneira DB , Gabrilovich DI , Kim ET , Syntaphilin controls a mitochondrial rheostat for proliferation-motility decisions in cancer. J Clin Invest 2017;127:3755–6928891816

18. Cox J , Mann M . MaxQuant enables high peptide identification rates, individualized p.p.b.-range mass accuracies and proteome-wide protein quantification. Nat Biotechnol 2008;26:1367–7219029910

19. Winter MR , Fang C , Banker G , Roysam B , Cohen AR . Axonal transport analysis using Multitemporal Association Tracking. Int J Comput Biol Drug Des 2012;5:35–4822436297

20. Wait E , Winter M , Bjornsson C , Kokovay E , Wang Y , Goderie S , Visualization and correction of automated segmentation, tracking and lineaging from 5-D stem cell image sequences. BMC Bioinformatics 2014;15:32825281197

21. Winter Mark R , Liu M , Monteleone D ,Melunis J , Hershberg U , Goderie Susan K , Computational Image Analysis Reveals Intrinsic Multigenerational Differences between Anterior and Posterior Cerebral Cortex Neural Progenitor Cells. Stem Cell Reports 2015;5:609–2026344906

22. Winter M , Mankowski W , Wait E , Temple S , Cohen AR . LEVER: software tools for segmentation, tracking and lineaging of proliferating cells. Bioinformatics 2016

23. Chenouard N , Smal I , Chaumont F , Maška M , Sbalzarini IF , Gong Y , Objective comparison of particle tracking methods. Nat Methods 2014;11

24. Thevenaz P , Ruttimann UE , Unser M . A pyramid approach to subpixel registration based on intensity. IEEE Trans Image Process 1998;7:27–4118267377

25. Wagner SA , Beli P , Weinert BT , Scholz C , Kelstrup CD , Young C , Proteomic analyses reveal divergent ubiquitylation site patterns in murine tissues. Mol Cell Proteomics 2012;11:1578–8522790023

26. Jung JU , Ravi S , Lee DW , McFadden K , Kamradt ML , Toussaint LG , NIK/MAP3K14 Regulates Mitochondrial Dynamics and Trafficking to Promote Cell Invasion. Curr Biol 2016;26:3288–30227889261

27. Campello S , Lacalle RA , Bettella M , Manes S , Scorrano L , Viola A . Orchestration of lymphocyte chemotaxis by mitochondrial dynamics. J Exp Med 2006;203:2879–8617145957

28. Ballinger CA , Connell P , Wu Y , Hu Z , Thompson LJ , Yin LY , Identification of CHIP, a novel tetratricopeptide repeat-containing protein that interacts with heat shock proteins and negatively regulates chaperone functions. Mol Cell Biol 1999;19:4535–4510330192

29. Birsa N , Norkett R , Wauer T , Mevissen TE , Wu HC , Foltynie T , Lysine 27 ubiquitination of the mitochondrial transport protein Miro is dependent on serine 65 of the Parkin ubiquitin ligase. J Biol Chem 2014;289:14569–8224671417

30. Connell P , Ballinger CA , Jiang J , Wu Y , Thompson LJ , Hohfeld J , The co-chaperone CHIP regulates protein triage decisions mediated by heat-shock proteins. Nat Cell Biol 2001;3:93–611146632

31. Murata S , Minami Y , Minami M , Chiba T , Tanaka K . CHIP is a chaperone-dependent E3 ligase that ubiquitylates unfolded protein. EMBO Rep 2001;2:1133–811743028

32. Tawo R , Pokrzywa W , Kevei E , Akyuz ME , Balaji V , Adrian S , The Ubiquitin Ligase CHIP Integrates Proteostasis and Aging by Regulation of Insulin Receptor Turnover. Cell 2017;169:470–82 e1328431247

33. Shang Y , He J , Wang Y , Feng Q , Zhang Y , Guo J , CHIP/Stub1 regulates the Warburg effect by promoting degradation of PKM2 in ovarian carcinoma. Oncogene 2017;36:4191–20028346425

34. Sarkar S , Brautigan DL , Parsons SJ , Larner JM . Androgen receptor degradation by the E3 ligase CHIP modulates mitotic arrest in prostate cancer cells. Oncogene 2014;33:26–3323246967

35. Wang Y , Ren F , Wang Y , Feng Y , Wang D , Jia B , CHIP/Stub1 functions as a tumor suppressor and represses NF-kappaB-mediated signaling in colorectal cancer. Carcinogenesis 2014;35:983–9124302614

36. Kajiro M , Hirota R , Nakajima Y , Kawanowa K , So-ma K , Ito I , The ubiquitin ligase CHIP acts as an upstream regulator of oncogenic pathways. Nat Cell Biol 2009;11:312–919198599

37. Radovanac K , Morgner J , Schulz JN , Blumbach K , Patterson C , Geiger T , Stabilization of integrin-linked kinase by the Hsp90-CHIP axis impacts cellular force generation, migration and the fibrotic response. EMBO J 2013;32:1409–2423612611

38. McDonough H , Charles PC , Hilliard EG , Qian SB , Min JN , Portbury A , Stress-dependent Daxx-CHIP interaction suppresses the p53 apoptotic program. J Biol Chem 2009;284:20649–5919465479

39. Ronnebaum SM , Wu Y , McDonough H , Patterson C . The ubiquitin ligase CHIP prevents SirT6 degradation through noncanonical ubiquitination. Mol Cell Biol 2013;33:4461–7224043303

40. Komander D , Rape M . The ubiquitin code. Annu Rev Biochem 2012;81:203–2922524316

41. Keating SE , Bowie AG . Role of non-degradative ubiquitination in interleukin-1 and toll-like receptor signaling. J Biol Chem 2009;284:8211–518684710

42. Wang W , Cantos-Fernandes S , Lv Y , Kuerban H , Ahmad S , Wang C , Insight into microtubule disassembly by kinesin-13s from the structure of Kif2C bound to tubulin. Nat Commun 2017;8:7028694425

43. Bouchet BP , Noordstra I , van Amersfoort M , Katrukha EA , Ammon YC , Ter Hoeve ND , Mesenchymal Cell Invasion Requires Cooperative Regulation of Persistent Microtubule Growth by SLAIN2 and CLASP1. Dev Cell 2016;39:708–2327939686

44. Watanabe T , Kakeno M , Matsui T , Sugiyama I , Arimura N , Matsuzawa K , TTBK2 with EB1/3 regulates microtubule dynamics in migrating cells through KIF2A phosphorylation. J Cell Biol 2015;210:737–5126323690

45. Mukherjee R , Majumder P , Chakrabarti O . MGRN1-mediated ubiquitination of alpha-tubulin regulates microtubule dynamics and intracellular transport. Traffic 2017;18:791–80728902452

46. Turnbull AP , Ioannidis S , Krajewski WW , Pinto-Fernandez A , Heride C , Martin ACL , Molecular basis of USP7 inhibition by selective small-molecule inhibitors. Nature 2017;550:481–629045389

47. Youle RJ , van der Bliek AM . Mitochondrial fission, fusion, and stress. Science 2012;337:1062–522936770

48. Senft D , Ronai ZA . Regulators of mitochondrial dynamics in cancer. Curr Opin Cell Biol 2016;39:43–5226896558

49. Ji WK , Hatch AL , Merrill RA , Strack S , Higgs HN . Actin filaments target the oligomeric maturation of the dynamin GTPase Drp1 to mitochondrial fission sites. Elife 2015;4:e1155326609810

50. Morita M , Prudent J , Basu K , Goyon V , Katsumura S , Hulea L , mTOR Controls Mitochondrial Dynamics and Cell Survival via MTFP1. Mol Cell 2017;67:922–35 e528918902

Author Manuscript

Author Manuscript

Author Manuscript

Author Manuscript

SIGNIFICANCE

Findings reveal a new mechanism of metastasis suppression by establishing the role of SNPH ubiquitination in inhibiting mitochondrial dynamics, chemotaxis and metastasis.
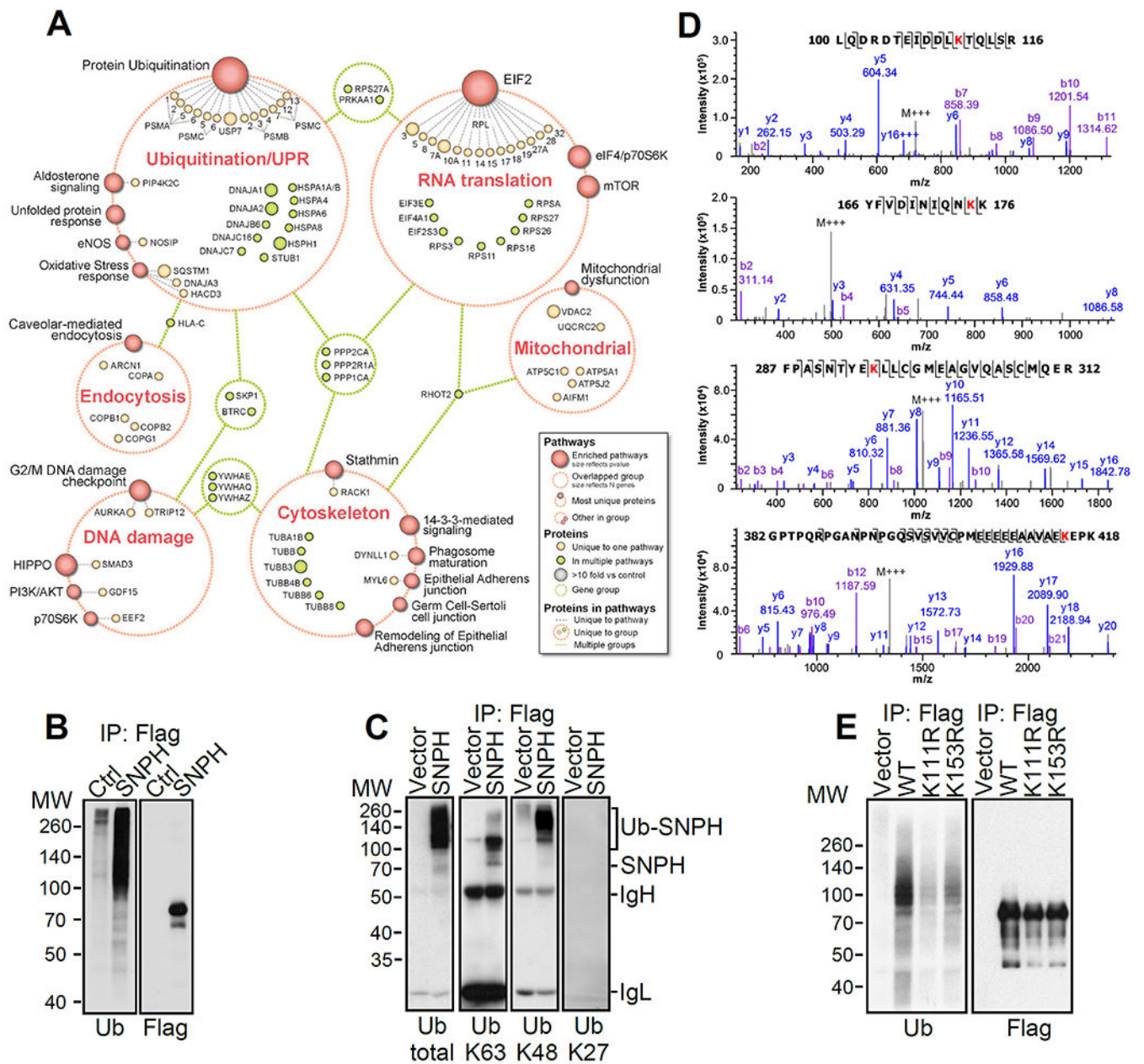
Figure 1.

SNPH ubiquitination. **A,** Bioinformatics pathway analysis of SNPH-associated proteins. PC3 cells transfected with vector or Flag-SNPH in duplicate, were immunoprecipitated with an antibody to Flag and co-associated proteins were identified by proteomics. The six most enriched pathways in SNPH-associated proteins are indicated. Pathways are represented by red filled circles, with area proportional to -log10 p value (larger circles represent more significant enrichment). Pathways sharing at least 50% proteins were combined into groups shown as dotted red circles with size proportional to total number of proteins in the pathway group. Unique (orange) and shared (green) proteins are indicated. **B,** Transfected PC3 cells were immunoprecipated (IP) with an antibody to Flag and analyzed with an antibody to

ubiquitin (Ub) or Flag, by Western blotting. **C,** The experimental conditions are as in **B,** except that Flag immunoprecipitates were analyzed with antibodies to the indicated ubiquitin (Ub) linkages. **D,** MS/MS spectra of identified ubiquitinated SNPH peptides. Ubiquitinated Lys residues are indicated in red. Identified b- and y-ions are indicated by horizontal bars above and below the sequence, respectively. M+++ denotes the triply charged precursor ion. **E,** PC3 cells were transfected with vector, Flag-wild type (WT) SNPH or Flag-SNPH mutant K111R or K135R, immunoprecipitated (IP) with an antibody to Flag and analyzed with an antibody to ubiquitin (Ub) or Flag, by Western blotting.
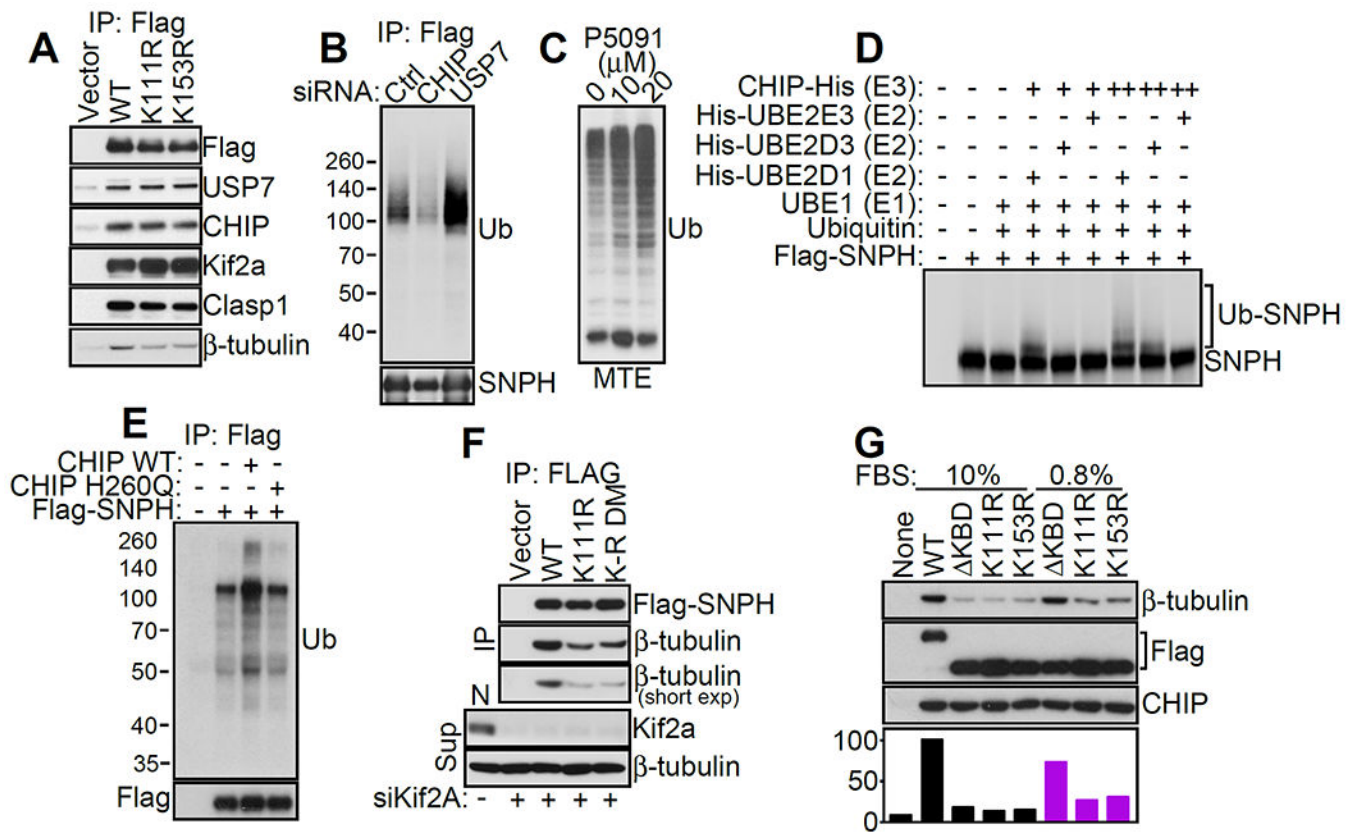
Figure 2.
Non-degradative SNPH ubiquitination regulates tubulin binding. **A,** PC3 cells transfected with vector, Flag-WT SNPH or Flag-SNPH mutant K111R or K153R were immunoprecipitated (IP) with an antibody to Flag, and co-associated proteins were analyzed by Western blotting. **B,** PC3 cells expressing Flag-SNPH were transfected with control non-targeting siRNA (Ctrl) or CHIP- or USP7-directed siRNA, immunoprecipitated (IP) with an antibody to Flag and immune complexes were analyzed with an antibody to ubiquitin (Ub) or SNPH, by Western blotting. **C,** PC3 cells were treated with the small molecule USP7 inhibitor, P5091 (0–20 μM) and isolated mitochondrial extracts were analyzed with an antibody to ubiquitin (Ub), by Western blotting. **D,** Recombinant CHIP (+, 1 μM; ++, 2 μM) was mixed with the indicated recombinant proteins in an in vitro ubiquitination reaction for 1 h at 37°C followed by Western blotting. The position of ubiquitinated (Ub) SNPH bands is indicated. **E,** PC3 cells were transfected with WT CHIP, CHIP mutant H260Q in the presence or absence of Flag-SNPH, immunoprecipitated (IP) with an antibody to Flag under serum-deprived conditions (0.8% FBS for 16 h) and analyzed by Western blotting. **F,** PC3 cells transfected with Kif2a-directed siRNA were reconstituted with vector, Flag-WT SNPH, Flag-SNPH mutant K111R or Flag-SNPH double mutant (DM) K111R/K153R, immunoprecipitated with an antibody to Flag, and proteins in immune complexes (IP) or supernatants (Sup) were analyzed by Western blotting. Short exp., short exposure. N, non-transfected. **G,** PC3 cells grown in 10% or 0.8% FBS for 16 h were transfected with vector, Flag-WT SNPH, Flag-SNPH mutant deleted in the kinesin-binding domain (KBD), Flag- KBD-K111R or Flag- KBD-K153R, and immune complexes precipitated with an
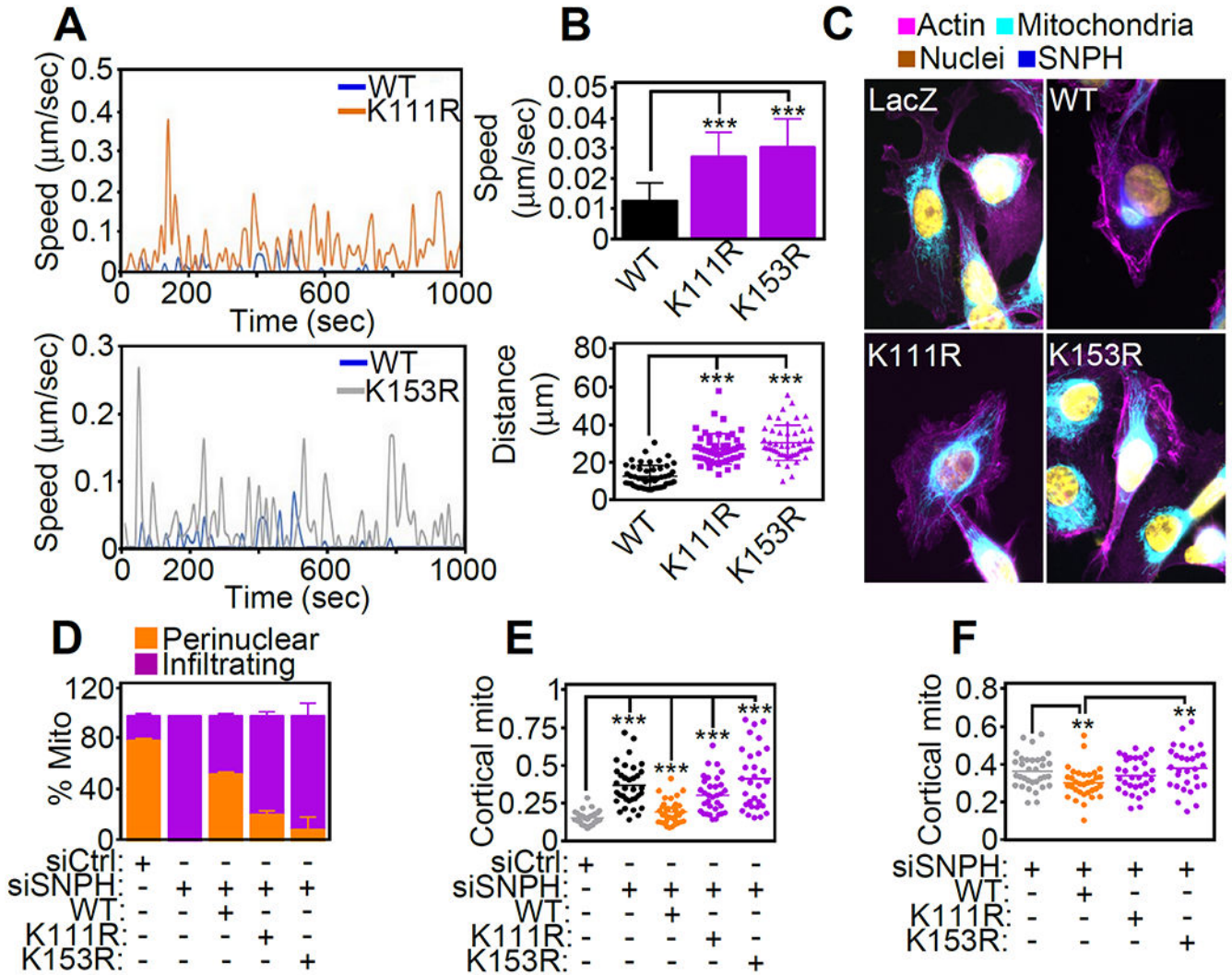
antibody to Flag were analyzed by Western blotting. Bar graph, densitometric quantification of tubulin bands.

Figure 3.

Regulation of mitochondrial trafficking by SNPH ubiquitination. **A,** Melanoma Yumm 1.7 cells were transfected with WT SNPH or SNPH mutant K111R (top) or K153R (bottom) and mitochondrial speed was quantified by time-lapse video microscopy. **B,** Melanoma Yumm 1.7 cells were transfected with WT SNPH or SNPH mutants K111R or K153R and changes in mitochondrial speed (top) or distance traveled by individual mitochondria (bottom) were quantified (n=50). ***, p<0.0001. **C,** PC3 cells silenced for endogenous SNPH by siRNA were transduced with LacZ or the indicated WT or mutant SNPH constructs and analyzed by fluorescence microscopy. **D,** The conditions are as in C, except that the percentage of mitochondria with perinuclear or cortical localization was quantified. Data are mean of replicates of a representative experiment. **E,** PC3 cells transfected with control non-targeted siRNA (siCtrl) or SNPH-directed siRNA (siSNPH) were reconstituted with WT SNPH or SNPH mutant K111R or K153R and analyzed for mitochondrial (mito) trafficking to the cortical cytoskeleton by time-lapse videomicroscopy. Data (n=31–34) are normalized per total mitochondrial mass. ***, p<0.0001. **F,** Yumm 1.7 cells were silenced

for endogenous SNPH by siRNA, reconstituted with control vector, WT SNPH or SNPH mutant K111R or K153R, and mitochondrial repositioning to the cortical cytoskeleton was quantified. Data are the mean±SD n=30–33). **, p=0.003–0.005.
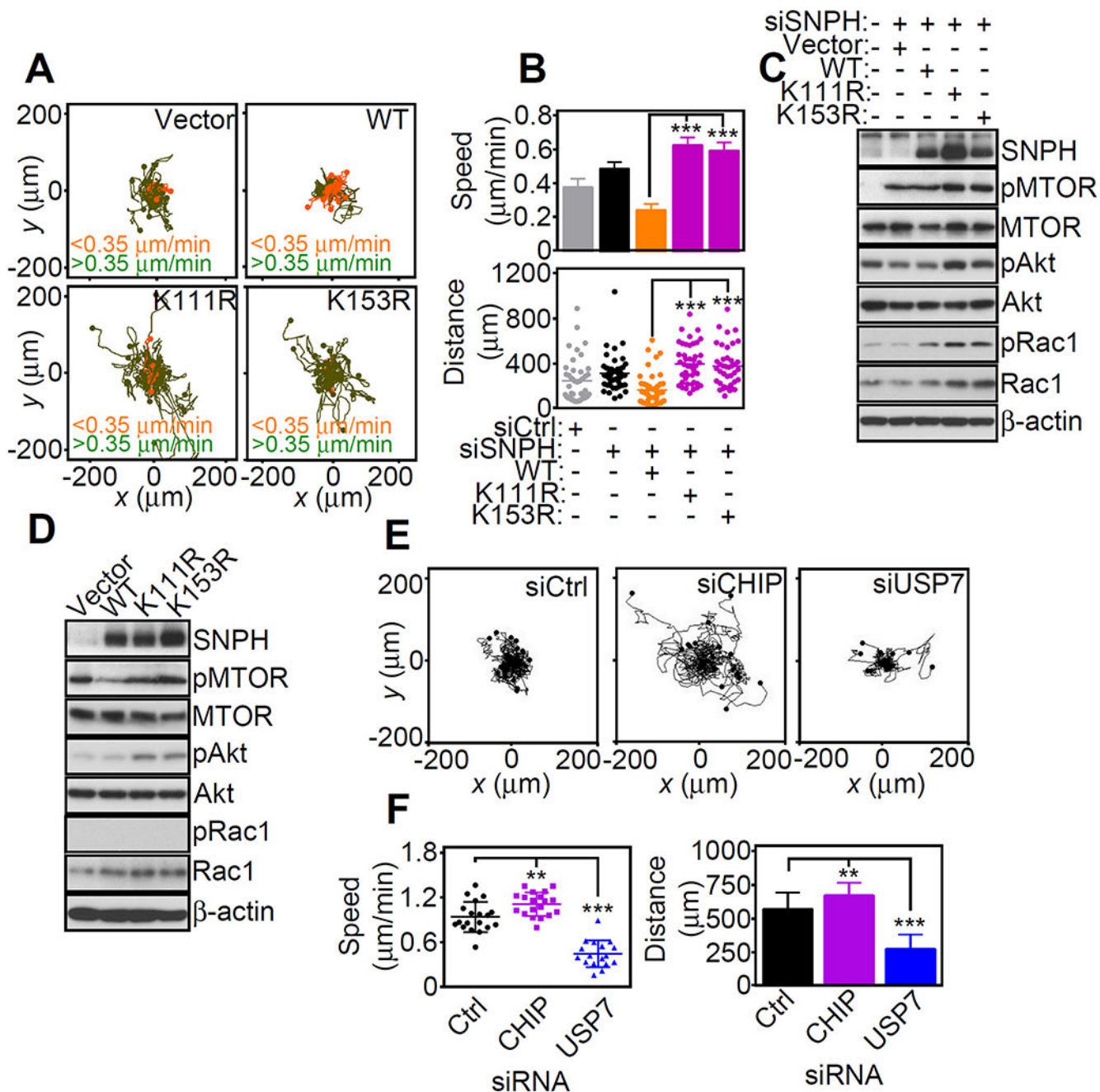
Figure 4.
SNPH ubiquitination regulates tumor chemotaxis. **A,** PC3 cells stably transduced with SNPH-directed shRNA (clone #0) were reconstituted with vector, WT SNPH or SNPH mutant K111R or K153R and analyzed for 2D chemotaxis by time-lapse video microscopy. Color-coded cutoff velocities of cell motility are indicated. Each tracing corresponds to an individual cell. **B,** The conditions are as in **A,** and shRNA-transduced PC3 cells reconstituted with the indicated plasmid constructs were analyzed for speed of cell migration (top, n=40–45) or total distance traveled by individual cells (bottom, n=40–45). Data are the

mean±SD. ***, p<0.0001. **C,** Yumm 1.7 cells transfected with vector, WT SNPH (WT) or SNPH mutants K111R or K153R were analyzed by Western blotting. p, phosphorylated. **D.** PC3 cells transfected with SNPH-directed siRNA were reconstituted with vector, WT SNPH or SNPH mutant K111R or K153R and analyzed by Western blotting. p, phosphorylated. **E** and **F,** PC3 cells transfected with the indicated siRNA were analyzed for 2D chemotaxis **E** and the speed of cell migration and distance traveled by individual cells (**F**) was quantified. Data are the mean±SD of replicates (n=17–19) of a representative experiment (n=2). **, p=0.006; ***, p<0.0001.
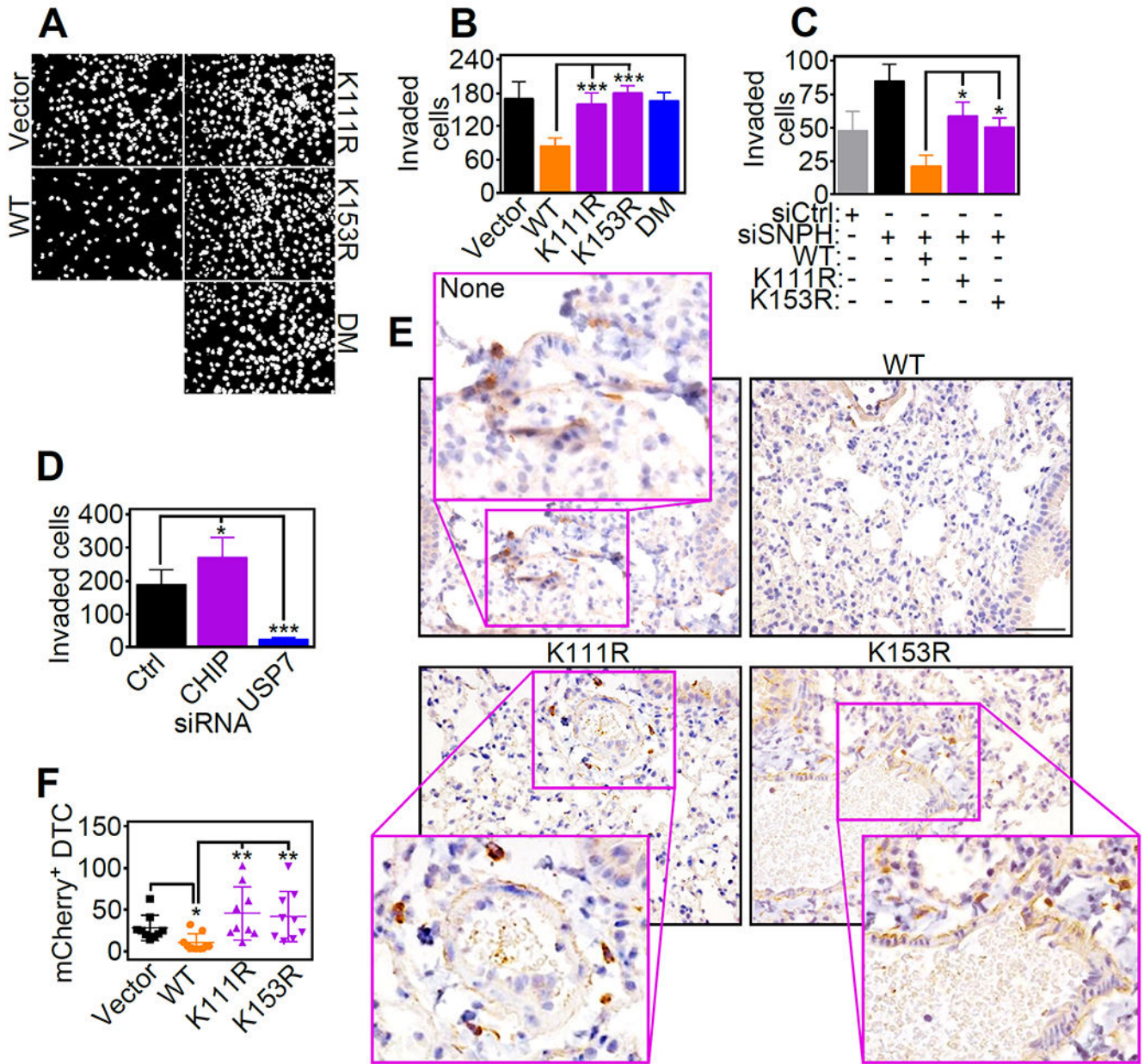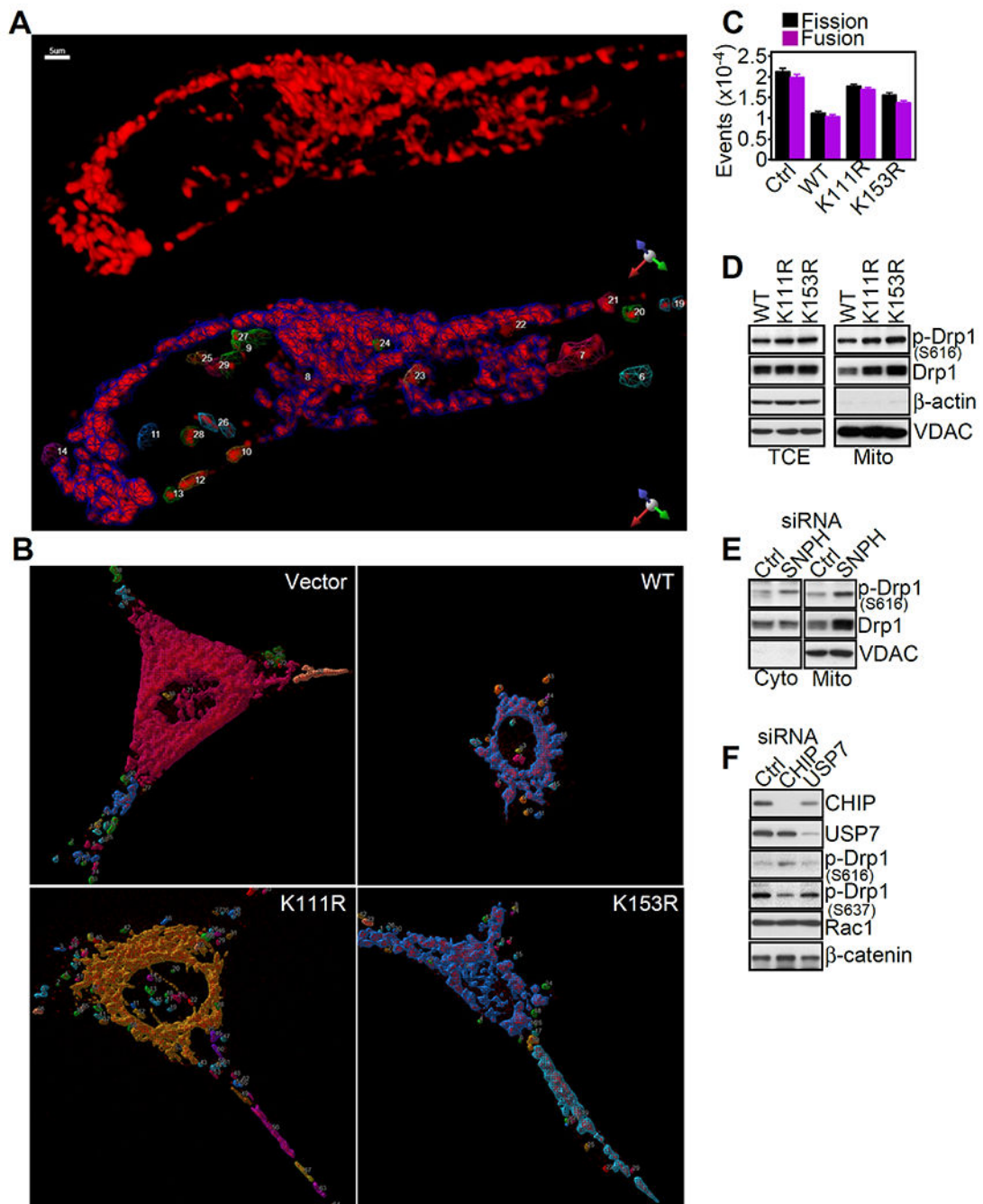
Figure 5.
Regulation of tumor cell invasion and metastasis by SNPH ubiquitination. **A,** PC3 cells transfected with vector, WT SNPH, SNPH mutant K111R or K153R or a SNPH double mutant (DM) K111R/K153R were analyzed for invasion across Matrigel-coated inserts and DAPI-stained nuclei of invaded cells were visualized by fluorescence microscopy. **B,** The conditions are as in **A,** and invaded cells were quantified. Data are the mean±SD of replicates of a representative experiment (n=3). p<0.0001. **C,** PC3 cells transfected with SNPH-directed siRNA were reconstituted with vector, WT SNPH or SNPH mutant K111R or K153R, and analyzed for Matrigel invasion. Data are the mean±SD of replicates of a representative experiment (n=3). *, p=0.02. **D,** PC3 cells transfected with the indicated siRNA were analyzed for Matrigel invasion. Data are the mean±SD of replicates of a

representative experiment (n=2). *, p=0.01; ***, p<0.0001. **E,** Yumm 1.7 cells expressing mCherrry and stably transfected with WT SNPH or SNPH mutant K111R or K153R were injected s.c. in syngeneic C57BL/6 mice and mCherry-positive cells disseminated to the lungs were detected by immunocytochemistry after 11 d. Scale bar, 50 μm. Inset, magnification of indicated regions (boxes). **F,** Quantification of mCherry-positive Yumm 1.7 cells in lungs of reconstituted animals (9 lungs per experimental group; 5–9 individual microscopy fields per condition). Each symbol corresponds to the mean number of disseminated tumor cells (DTC) per lung of an individual animal. *, p=0.01; **, p=0.006–0.009.

Figure 6.

Modulation of mitochondrial dynamics by SNPH ubiquitination. **A,** One frame of 82 from a confocal microscopy image sequence showing mitotracker-labeled mitochondria (top). Mitochondria are segmented in each frame and tracked throughout the image sequence (bottom). The colored mesh indicates the segmentation boundaries, with different colors and numeric labels assigned to different tracked mitochondria. Tracking results are used to identify fission and fusion events, with track initiation indicating mitochondrial fusion and track termination indicating mitochondrial fission events. **B,** Mitochondrial dynamics was

assessed by time-lapse videomicroscopy in Yumm 1.7 cells transfected with vector, WT SNPH or SNPH mutant K111R or K153R. Representative images of 3D rendering of individual cells per condition are shown. **C,** The conditions are as in **A** and **B,** and mitochondrial fusion and fission events/voxel/frame were calculated in Yumm 1.7 transfectants. Data are the mean±SEM (n=61 movies from 10 imaging experiments after deconvolution: Vector, 9 movies; WT SNPH, 20 movies; SNPH mutant K111R, 19 movies; SNPH mutant K154R, 13 movies). **D,** PC3 cells were transfected with WT SNPH or SNPH mutant K111R or K153R and total cell extracts (TCE) or mitochondrial (Mito) fractions were analyzed by Western blotting. **E,** PC3 cells were transfected with control non-targeting siRNA (Ctrl) or SNPH-directed siRNA and cytosol (Cyto) or mitochondrial (Mito) were extracts analyzed by Western blotting. **F,** PC3 cells were transfected with non-targeting siRNA (Ctrl) or CHIP- or USP7-directed siRNA and total cell extracts were analyzed by Western blotting. For **D-F**, antibodies to the different Drp1 phosphorylation (p) sites are indicated; p, phosphorylated.
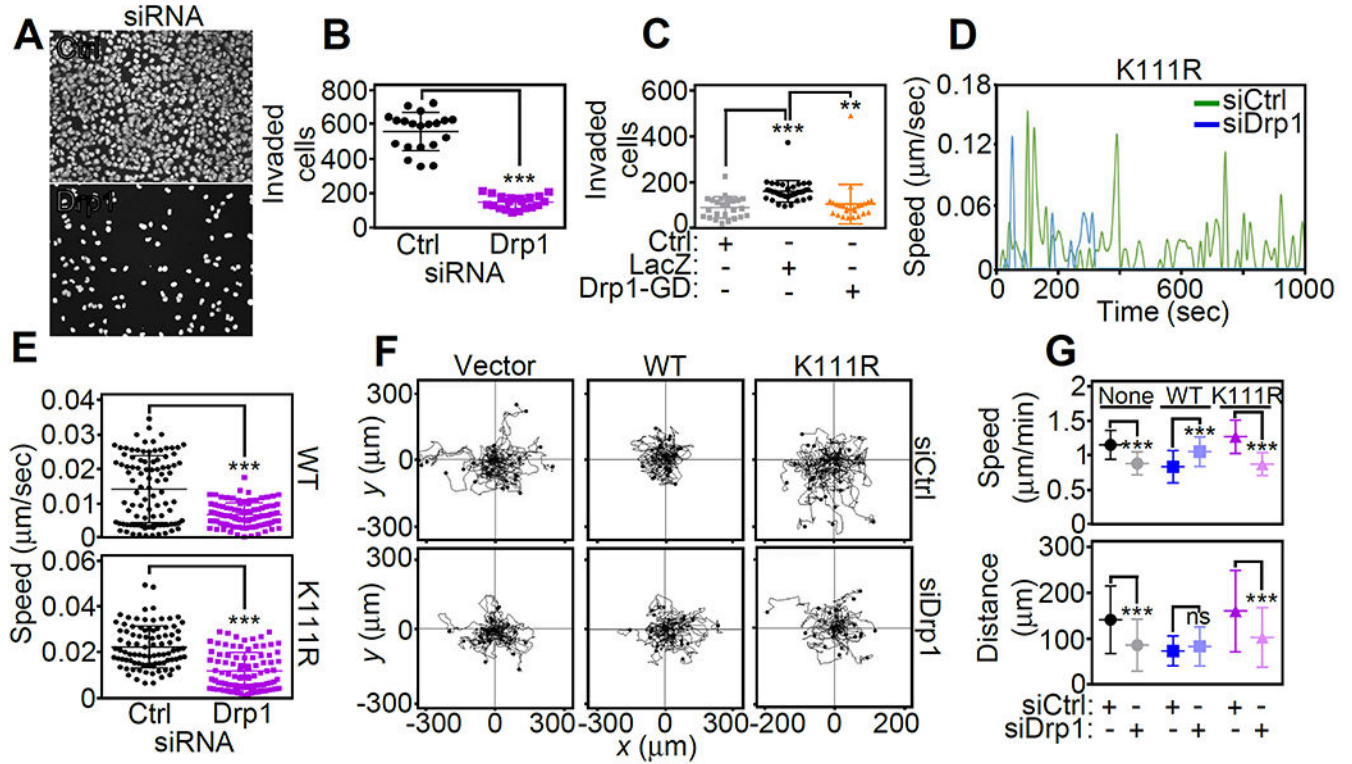
Figure 7.
Requirement of Drp1 for mitochondrial trafficking and tumor cell invasion. **A** and **B,** PC3 cells transfected with control non-targeting siRNA (Ctrl) or Drp1-directed siRNA were analyzed for Matrigel invasion and DAPI-stained nuclei of invaded cells were visualized by fluorescence microscopy (**A**) and quantified (**B**). Data are the mean±SD (n=3). ***, p<0.0001. **C,** PC3 cells stably transduced with SNPH-directed shRNA or control shRNA were reconstituted with vector or Drp1 GTPase-mutant cDNA (Drp1-GD), and analyzed for Matrigel invasion. Data are the mean±SD (n=3). **, p=0.001; ***, p<0.0001. **D,** Yumm 1.7 cells stably expressing SNPH mutant K111R were reconstituted with control non-targeting siRNA (Ctrl) or Drp1-directed siRNA and the speed of mitochondrial movements was quantified by time-lapse videomicroscopy. **E,** The conditions are as in **D,** except that the speed of individual mitochondrial movements (n=49–50) was quantified for Yumm 1.7 cells reconstituted with WT-SNPH (top) or SNPH mutant K111R (bottom). Each point corresponds to an individual mitochondrial track. ***, p<0.0001. **F** and **G,** Yumm 1.7 cells stably expressing vector, WT SNPH or SNPH mutant K111R were transfected with control non-targeting siRNA (Ctrl) or Drp1-directed siRNA and analyzed for 2D-chemotaxis (**F**) with quantification of speed of cell motility (top) and distance traveled by individual cells (bottom) (**G**). Data are the mean±SD (n=19–21). **, p=0.001; ***, p<0.0001. In **F,** each tracing corresponds to an individual cell.